Approximate time-dependent current-voltage relations for currents exceeding the diffusion limit

Yoav Green*

Department of Mechanical Engineering, Ben-Gurion University of the Negev, Beer-Sheva 8410501, Israel

(Received 24 February 2020; accepted 6 April 2020; published 29 April 2020)

The time-dependent behavior of one-dimensional ion transport into a permselective medium is theoretically modeled in this work for currents exceeding the diffusion limit. Leveraging the findings of Yariv [E. Yariv, Phys. Rev. E **80**, 051201 (2009)], we derive three separate expressions for the potential drop for short, intermediate, and long times. We show that the potential drop correlates to the time evolution of the space-charge layer adjacent to the permselective interface. Our approximate models show remarkable correspondence to numerical simulations.

DOI: 10.1103/PhysRevE.101.043113

I. INTRODUCTION

Ion transport through permselective media is prevalent in nature and technology. Desalination through electrodialysis [1–4] and energy harvesting in reverse electrodialysis [5–10] rely on large membranes that separate or mix electrolytes of different concentration. Biosensors [11–13], fluid based electrical diodes [7,14–19], and various physiological phenomena [20] utilize either permselective nanochannels or permselective nanopores for their respective functions. Yet, despite its importance, the fundamental physics of ion transport through permselective media has yet to be fully revealed. This can be attributed to the difficulty in analyzing the nonlinear coupled set of equations governing ion transport.

Fortunately, in recent decades much progress has been made, notably, in understanding the steady-state response. In contrast to time-dependent processes, steady-state responses are easier to mathematically model, as well as easier to interpret experimentally. For example, in the steady state, ion transport is characterized by a current-density-voltage (i-V) response curve which has three different regions (Fig. 1).The first region, termed the Ohmic response, is the low voltage response characterized by a linear resistance, $R = V/i$ [21]. The second region, termed the limiting current response, occurs at intermediate voltages when the current saturates to a diffusion limiting value, $i_{\rm lim}$. The third region termed the overlimiting current (OLC) response, $i_{\rm OLC}$, occurs above a critical voltage value where nonlinear effects dominate. In contrast to the steady state, time-dependent responses are more involved, mathematically, and thus less understood. In this work, we address transient effects in simple one-dimensional (1D) systems.

In 1D systems, it has long been known that the (nondimensional) convectionless i-V response is given by [1,22,23] (see Sec. II for normalizations of the current and voltage)

$$i = 2(1 - e^{-V/2}). \tag{1}$$

The diffusion limited current saturates to a limiting value $i_{\rm lim} = 2$. However, Rubinstein and Shtilman [23] showed that this diffusion limited current could be surpassed with the formation of a nonequilibrium extended space-charge layer (eSCL) at the permselective interface. Through numerical simulations, they showed that the current increased linearly with the normalized electric double layer (EDL) parameter, ε, which will be defined later (see Fig. 2). These above-limiting currents are related to the overlimiting currents, $i_{\rm OLC}$, but at the same time they are different. In the remainder, we will mark a distinction between these two. We will denote these above-limiting (AL) currents as $i_{\rm AL}$. The reason for this is primarily semantics. In works focusing on OLCs, an additional physical mechanism is required for $i_{\rm OLC}$. For example, Rubinstein and Zaltzman [4,24,25] showed that at sufficiently high voltages the eSCL is unstable and results in electroconvective effects that are responsible for $i_{\rm OLC}$. Thus, $i_{\rm OLC}$ is a natural extension of $i_{\rm AL}$ with the appearance of electroconvection [26,27]. This is also true for $i_{\rm OLC}$ due to surface conductance [28], water splitting [29–31], and more. However, in this work we do not address any of these OLC

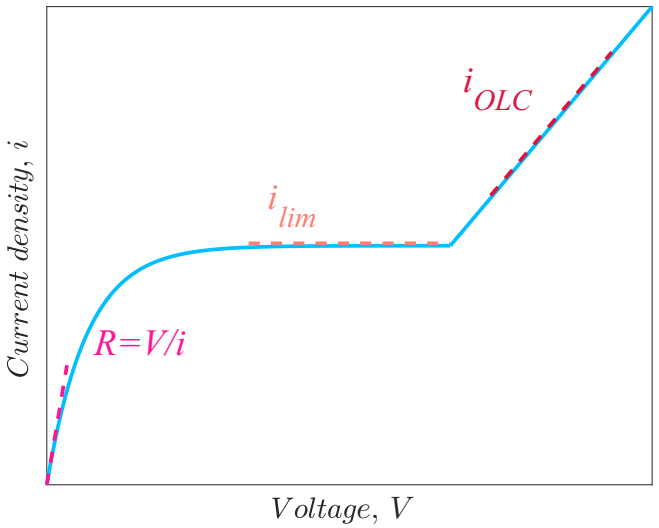

FIG. 1. The current-voltage, i-V, response comprises three regions: linear Ohmic resistance, R; limiting current, $i_{\rm lim}$; and overlimiting current, $i_{\rm OLC}$.

*yoavgreen@bgu.ac.il

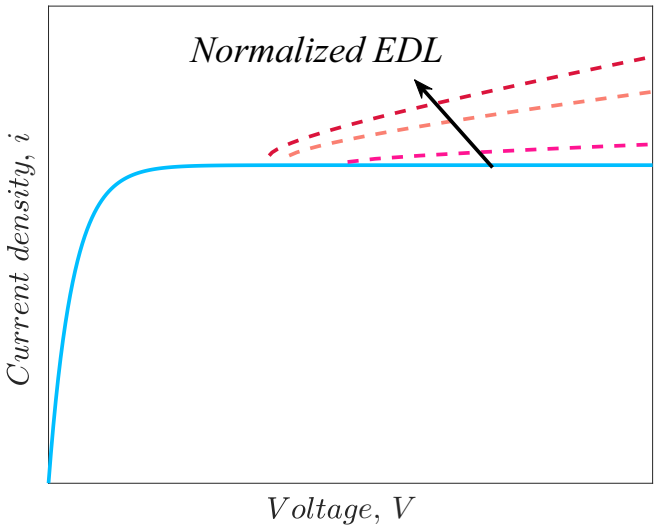

FIG. 2. Schematic of current-voltage relation surpassing the limiting currents. The solid blue line is given by Eq. (1) while dashed lines with increasing ε are determined by Eq. (41).

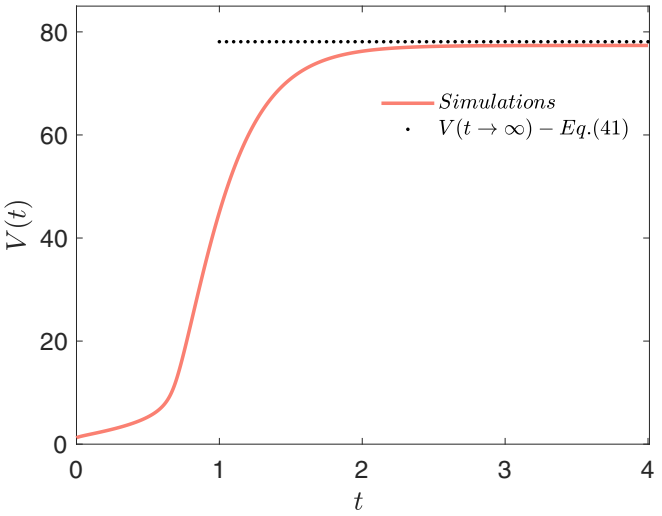

FIG. 3. Time evolution of the potential drop similar to what was shown in Ref. [42] but with different simulation parameters (as given in Fig. 6).

mechanisms; rather we focus solely on the effects of the eSCL to produce these above-limiting currents.

The peculiar behavior of the steady state i_{AL}-V has been addressed in a number of works. Rubinstein and Shtilman [23] were the first to demonstrate the existence of i_{AL} via numerical simulations. Later Ben and Chang [32] were the first to derive an approximation for i_{AL}-V for large voltages. This work would later serve as the basis for the equation derived in Yossifon *et al.* [33] and used to explain experimental observations of above-limiting currents. In later works, Chu and Bazant [34,35] derived asymptotic expressions for above-limiting currents. Similarly, Yariv [36,37] addressed the issue of the potential drop across the entire layer (dotted black line in Fig. 3). It should be noted that the common feature of all these works is that they focused on the steady-state solution and ignored transition effects. In this work, we will use much of Yariv's [36] formulation and we denote this work as Y09.

Yet others have been studying the time evolution of these effects. Due to the inherent complications, most of the theoretical work focused on the limiting case of $\varepsilon \to 0$ whereby the governing equations are drastically simplified [38–41]. Others have addressed time-dependent problems in concordance with other overlimiting mechanisms while the time dependency of the eSCL has yet to be addressed [42–44]. Most recently, Abu-Rjal *et al.* [42] considered the important question of how the electroconvective dominated potential drop deviates from the expected convectionless response. Their focus was electroconvection; however, their numerical results presented an equally interesting and overlooked question which served as inspiration for this work—why does the convectionless response behave as it does (solid line in Fig. 3)? In other words, what is the time-dependent current-voltage response for above-limiting currents $[V(t, i_{\mathrm{AL}})]$?

This work addresses the time-dependent current-voltage response $V(t, i_{\mathrm{AL}})$. Section II presents the governing equations and discusses the characteristic behavior of steady-state ion transport. Transient effects are also discussed. Notably, using numerical simulations we demonstrate how the structure of the extended space-charge layer varies for these different scenarios. In Sec. III, leveraging the findings of Y09 we present the $V(t, i_{\mathrm{AL}})$ relations for short times, intermediate times, and steady state. Concluding remarks are given in Sec. IV.

II. THEOERTICAL MODEL

A. Governing equations

The one-dimensional (1D) equations governing the time-dependent transport of a symmetric and binary ($z_+ = -z_- = 1$) electrolyte of equal diffusivities ($D_+ = D_- = D$) through a permselective medium are the dimensionless Poisson-Nernst-Planck (PNP) equations:

$$c^+_{,t} = c^+_{,xx} + (c^+\phi_{,x})_{,x} = -j^+_{,x}, \tag{2}$$

$$c^-_{,t} = c^-_{,xx} - (c^-\phi_{,x})_{,x} = -j^-_{,x}, \tag{3}$$

$$2\varepsilon^2\nabla^2\phi = -(c^+ - c^-). \tag{4}$$

Equations (2) and (3) are the Nernst-Planck equations satisfying continuity of ionic fluxes for the cation and anion concentrations c^+ and c^-, respectively. The current densities $j_\pm$ are given accordingly by Eqs. (2) and (3). Equation (4) is the Poisson equation for the electric potential. The concentrations have been normalized by their bulk value c_0. The electric potential has been normalized by the thermal potential $\phi_{th} = \Re T/F$ where $\Re$, T, and F are the universal gas constant, absolute temperature, and Faraday constant, respectively. The current densities have been normalized by Dc_0L^{-1} where D is the diffusion coefficient and L is the length of the system. Space and time have been normalized by L and L^2/D, respectively. These lead to the definition of the normalized EDL,

$$\varepsilon = \frac{\lambda_D}{L}, \quad \lambda_D = \sqrt{\frac{\varepsilon_0\varepsilon_r\Re T}{2F^2c_0}}, \tag{5}$$

where ε_0 and ε_r are the permittivity of vacuum and the relative permittivity of the electrolyte, respectively, and λ_D is the Debye length. Finally, it should be noted that the electrical current density i is normalized by FDc_0L^{-1} [7,45].

B. Boundary conditions

Equations (2)–(4) govern ion transport in a 1D system such as the one shown in Fig. 5. In this 1D domain, the bulk region is defined at $x = 1$. There we have the standard bulk boundary condition (BC) on the concentration and zero potential:

$$c^{\pm}(x = 1, t) = 1, \tag{6}$$

$$\phi(x = 1, t) = 0. \tag{7}$$

At the ideal permselective interface at $x = 0$ we have

$$c^{+}(x = 0, t) = N, \quad j^{-}(x = 0, t) = 0, \tag{8}$$

$$\phi = -V - \ln N. \tag{9}$$

The first term in Eq. (8) is the requirement that the counterion concentration equals that of membrane. The second term in Eq. (8) ensures that the coion flux is zero. Equation (9) is a condition that the total potential drop over the system is V. The $\ln N$ term has been added to ensure that for zero voltages, the current is zero. As we are interested in the time evolution of the concentration, initial conditions are needed, which are that everywhere outside of the thin EDL of order $O(\varepsilon)$ the bulk is electroneutral and is unity:

$$c^{\pm}(x, t = 0) = 1. \tag{10}$$

In steady state this approach, known as the potentiostatic approach, dictates the potential drop across the system from which the electrical current density is calculated. However, as pointed out by others [24,32,33,35,36,39,45] the reverse galvanostatic approach (input the current and calculate the potential drop) is much easier for theoretical modeling. This argument of potentiostatic versus galvanostatic also holds for time-dependent problems and we adopt the latter. Thus, we replace Eqs. (7) and (9) with two modified BCs,

$$\phi_{,x}(x = 1, t) = -\tfrac{1}{2}i, \tag{11}$$

$$\phi = -\ln N, \tag{12}$$

where we dictate the current and calculate the potential drop across the system.

C. Numerical simulations

Numerical simulations of the fully coupled Poisson-Nernst-Planck equations [Eqs. (2)–(4)] with the appropriate BCs [Eqs. (6),(8),(11), and (12)] were conducted in COMSOL using the Transport of Diluted Species and Electrostatics modules for both the time-dependent and time-independent scenarios. The various simulation parameters are given in the figures below. See previous works for more details [7,19,45] regarding simulations.

D. Steady-state distributions

In Figs. 4(a) and 4(b) we plot the steady-state positive charge-carrier concentration and space-charge distributions $q = \frac{1}{2}(c^{+} - c^{-})$ [Eq. (14)], respectively, calculated from numerical simulations for a number of different currents.

At low currents, $i < i_{\text{lim}}$, it can be observed that the concentration profile has a minimum near $x = 0$ while the space-charge distribution has an almost equilibrium profile (similar to that of $i = 0$). For $i < i_{\text{lim}}$, the changes in the concentration and space charge are limited to two regions: (1) the diffusion layer (DL), $x \in (O(\varepsilon^{2/3}), 1]$; (2) the cathodic boundary layer (CBL), $x \in [0, O(\varepsilon^{2/3}))$. The scaling for the DL, CBL, and two more regions defined below are discussed thoroughly in Y09. We note that in the 1D steady state the DL

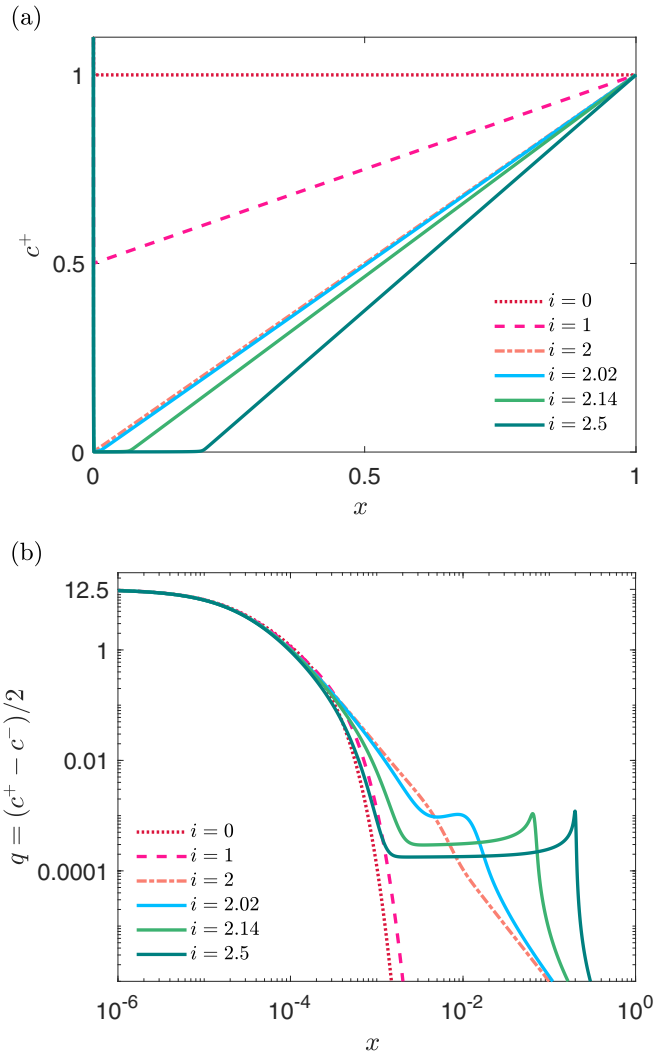

FIG. 4. Steady-state profiles for (a) the positive concentration distribution, c^{+}, and (b) the space-charge density, q [Eq. (14)], for various currents. Simulation parameters are $\varepsilon = 10^{-4}$, $N = 25$. For presentation purposes in (a) we show concentration in the range of 0–1 but note that there is a boundary layer near $x = 0$ such that $c^{+}(x = 0) = N$. In (b) which is a log-log plot, we show that the space charge is primarily dominated by the positive charge carrier such that $q(x = 0) \approx \frac{1}{2}c^{+}(x = 0) = N/2$.

is characterized by a linear change in the concentration of both positive and negative charge carriers. In contrast, in the CBL the negative and positive concentrations behave differently. The positive concentration drops from a very high concentration $c^+(x=0)=N$ to the value of the concentration in the DL, within a length of $O(\varepsilon^{2/3})$. For small ε, this implies that a boundary layer exists near $x=0$, as shown in Fig. 4(a). The negative concentration rises from a value that is of $O(N^{-1})$ to its value in the DL. This difference between positive and negative charge carriers gives rise to the space-charge density q [Fig. 4(b)].

As the current increases, $i \approx i_{\rm lim}$, we notice that the linear concentrations profile reaches a minimum at the point $\tilde{x}_* = x \neq 0$ (which will be defined later). A third region, denoted as the space-charge layer (SCL), appears between the DL and the CBL. In this region the concentrations are near zero. This region is commonly known as the depleted region. Now the DL is limited to the region $x \in (x_*, 1]$. The SCL is defined in the region, $x \in (O(\varepsilon^{2/3}), x_*)$. We later show that to leading order both the concentration and space-charge density in this region are of order ε. The extended space-charge layer (eSCL) now comprises both the CBL and the SCL. At even larger currents, $i = i_{\rm AL} > i_{\rm lim}$, we see that formation of a "small hump" in between the SCL and the DL. This fourth region, predicted by Zaltzman and Rubinstein [24,25], is called the transition layer (TL), which also has a length of $O(\varepsilon^{2/3})$. More information about this region can be found in Y09. Now the eSCL is comprised of three regions (CBL, SCL, and TL). To calculate the total potential drop across the system when $i = i_{\rm AL} > i_{\rm lim}$, one has to integrate the electric field across all four regions. This was cleverly done by Y09 and is discussed later in Sec. III C.

Depending on the current density, the steady state concentration and space-charge distributions can be divided into two to four regions. The number of regions depends on the current density, i. The length of each region depends both on the current density as well as the normalized EDL, ε. These regions are summarized in Fig. 5.

E. Time-dependent distributions

In Figs. 6(a) and 6(b) we plot the time-dependent positive charge-carrier concentration and space-charge distributions, respectively, calculated from numerical simulations for an above-limiting current density.

At early times, the concentration profiles are not spatially linear. The time evolution of the concentration is given later in Sec. III B. However, it can be observed that the space charge is at quasiequilibrium where the space-charge profile appears similar to the $t=0$ solution. For this situation, it appears that the space-charge layer comprises the electroneutral DL and charged CBL.

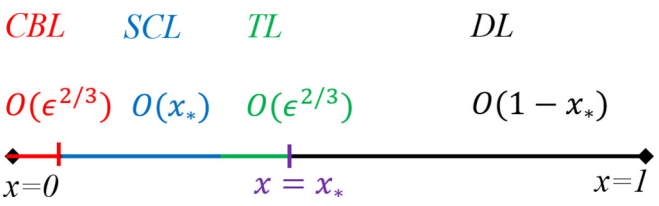

FIG. 5. A schematic of the 1D geometry within the domain $x \in [0, 1]$. The domain is divided into four regions: CBL, SCL, TL, and DL. The order of magnitude of the length of each region is given;see main text for more details (Sec. II D).

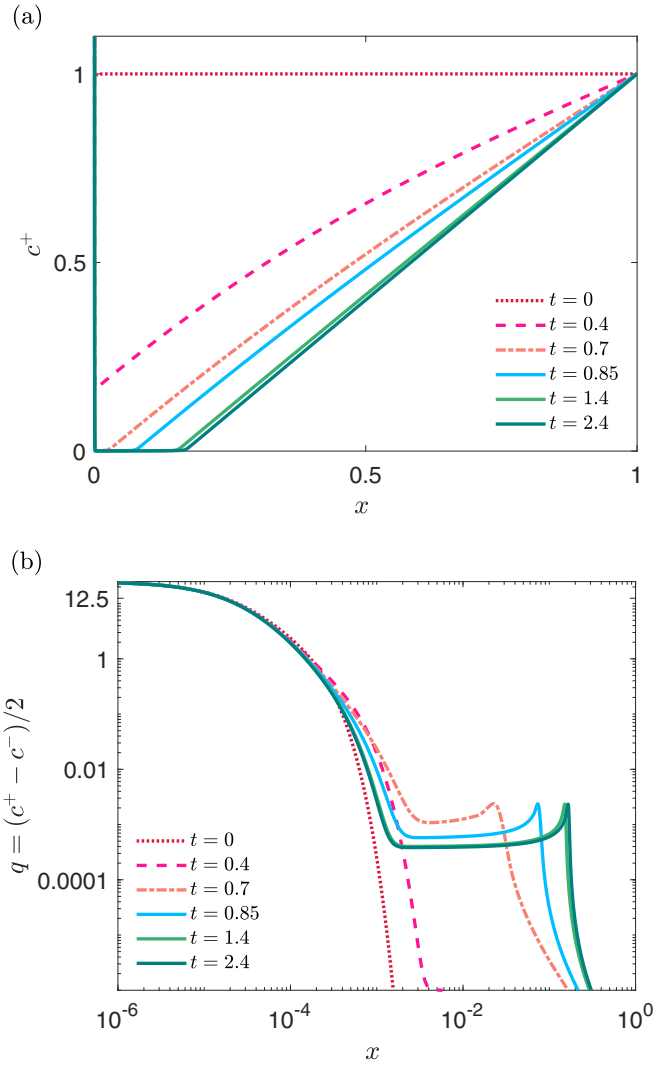

FIG. 6. Time-dependent profiles for (a) the positive concentration distribution, c^+, and (b) space-charge density, q, for different times. Simulation parameters are $\varepsilon = 10^{-4}$, $N = 25$, $i = 2.4$.

At intermediate times, when the profile is fully depleted at $x \approx 0$, it appears that the space-charge transitions to a region that includes both the SCL and the TL. Two observations are noteworthy. First, the SCL's length increases over time until it eventually reaches a steady state. Second, while the TL does appear it does not reach its final profile until later times. Later, we will make an ansatz, that for these intermediate times the effects of the TL are negligible.

Finally, at late times, the distributions appear to have reached their steady-state values and the structure of the space now comprises the four regions described in Sec. II D and shown in Fig. 5.

F. Analogies between steady-state and time-dependent space-charge distributions

There are obvious differences between time-dependent above-limiting current responses versus the steady-state response. However, Figs. 4 and 6 suggest that perhaps some fundamental aspects might be shared:

(1) For short times, before the concentrations are completely depleted, it appears that both above-limiting time-dependent problems and underlimiting steady-state problems are similar in that they both depend only on the DL and CBL.

(2) At intermediate times, when the depletion is still localized around $x \approx 0$ both the SCL and TL form. However, similar to the steady-state response for $i \approx i_{\rm lim}$, perhaps the TL is not completely formed and its effects are negligible.

(3) At large times, the time-dependent profiles reached are quasi steady state and are comprised of four regions.

III. SOLUTION

The three observations from Sec. II F will be used in this section to model the time-dependent behavior of the potential drop across the system, $V(t)$, for short, intermediate, and long times. We will show that using these assumptions, we can describe the behavior of the numerically calculated $V(t)$ (solid line in Fig. 7).

We start by reducing the mathematical complexity of the problem. We will then present the early times solution, after which we will present the steady-state solution of Y09. Thereafter, we will return to intermediate times.

A. Mathematical simplification

Here we reduce the number of governing equations from three to two. The electric field is related to the electric potential by

$$E = -\phi_{,x}. \tag{13}$$

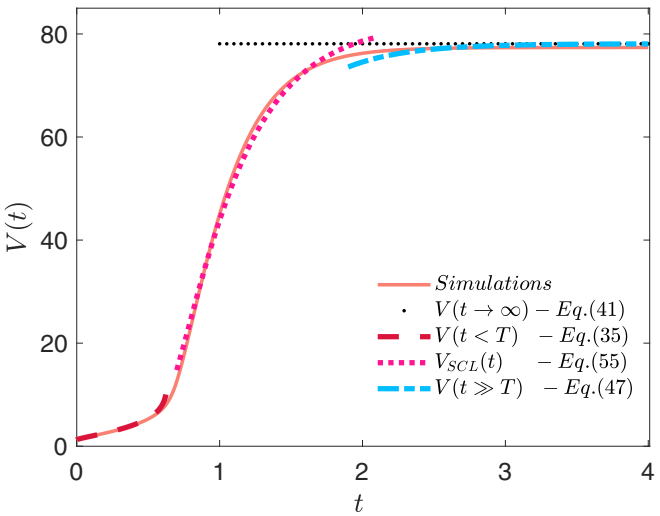

FIG. 7. Time evolution of the voltage, $V(t)$. Simulation parameters as in Fig. 6.

Also, the space-charge density q and average salt density c are defined as

$$q = \tfrac{1}{2}(c^+ - c^-), \tag{14}$$

$$c = \tfrac{1}{2}(c^+ + c^-). \tag{15}$$

Inserting Eqs. (13) and (14) into Eqs. (2)–(4) yields

$$c^+_{,t} = c^+_{,xx} - (c^+E)_{,x}, \tag{16}$$

$$c^-_{,t} = c^-_{,xx} + (c^-E)_{,x}, \tag{17}$$

$$\varepsilon^2 E_{,x} = q. \tag{18}$$

Taking the sum and difference of Eqs. (16) and (17) yields

$$c_{,t} = c_{,xx} - (qE)_{,x}, \tag{19}$$

$$q_{,t} = q_{,xx} - (cE)_{,x}. \tag{20}$$

Inserting Eq. (18) into Eqs. (19) and (20) yields

$$c_{,t} = c_{,xx} - \tfrac{1}{2}\varepsilon^2(E^2)_{,xx}, \tag{21}$$

$$\varepsilon^2 E_{,xt} = \varepsilon^2 E_{,xxx} - (cE)_{,x}. \tag{22}$$

Integrating Eq. (22) yields

$$-\varepsilon^2(E_{,t} - E_{,xx}) = cE + \text{const}. \tag{23}$$

Since this equation must also satisfy Eq. (11) to zeroth order in ε, we have that the constant equals $i/2$. Equations (21) and (23) are the governing equations.

B. Short times

Before the concentration near the depleted interface ($x = 0$) reaches zero the CBL is still quasiequilibrium. We consider the case where we have only two regions: CBL and DL. We will derive the DL solution while the effects of the EDL or CBL will be accounted as a BC—this approach is different than that of Y09 in which a boundary-layer approach was used to model the behavior of the CBL.

In the diffusion layer (DL) we consider a series expansions for the electric field:

$$E_{\rm DL} \approx E_{\rm DL,0} + \varepsilon E_{\rm DL,1} + \varepsilon^2 E_{\rm DL,2} + \cdots. \tag{24}$$

Equation (18) implies that to leading order $q \sim O(\varepsilon^2)$ and the concentration, to leading order, is also independent of ε. Thus, in the DL we can reduce the governing equations from

$$c_{,t} = c_{,xx} - \tfrac{1}{2}\varepsilon^2(E^2)_{,xx}, \tag{25}$$

$$-\varepsilon^2(E_{,t} - E_{,xx}) = cE + \tfrac{1}{2}i, \tag{26}$$

to

$$c_{\rm DL,t} = c_{\rm DL,xx}, \tag{27}$$

$$c_{\rm DL}E_{\rm DL,0} = -\tfrac{1}{2}i. \tag{28}$$

The time-dependent solution for Eq. (27), with the above dictated BCs, in the finite domain is given in Refs. [38,39,45],

$$c_{\rm DL}(x,t) = 1 - \frac{i}{2}(1-x) - i\sum_{m=1}^{\infty}\frac{(-1)^m}{\gamma_m^2}e^{-\gamma_m^2 t}\sin[\gamma_m(1-x)], \tag{29}$$

where the eigenvalues are given by

$$\gamma_m = \pi\left(m - \tfrac{1}{2}\right). \tag{30}$$

The potential drop over the entire region is

$$V = \Delta\phi = \Delta\phi_{\rm DL} + \Delta\phi_{\rm CBL} - \ln N, \tag{31}$$

where the last term accounts for the nonzero potential given in Eq. (12). The potential difference across the DL [utilizing Eq. (28)] is

$$\Delta\phi_{\rm DL}(t) = \int_0^1 \frac{\partial\phi}{\partial x}dx = -\int_0^1 E_{\rm DL}dx = \int_0^1 \frac{i}{2c_{\rm DL}(x,t)}dx. \tag{32}$$

The potential drop across the CBL can be calculated by requiring that the counterion electrochemical potential,

$$\mu = \ln c^+ + \phi, \tag{33}$$

is conserved at the interface located approximately at $x \cong \varepsilon \ll 1$. Hence we have

$$\Delta\phi_{\rm CBL}(t) = \phi(x=\varepsilon^+,t) - \phi(x=\varepsilon^-,t) = \ln\left[\frac{c^+(x=\varepsilon^-,t)}{c^+(x=\varepsilon^+,t)}\right] \cong \ln\left[\frac{N}{c_{\rm DL}(x=0,t)}\right]. \tag{34}$$

Using the notation that T is the time at which concentration at the permselective interface is zero is completely depleted [$c_{\rm DL}(x=0,t=T) \cong 0$], we find that the potential drop is

$$V(t<T) = \Delta\phi(t<T) = \int_0^1 \frac{i}{2c_{\rm DL}(x,t)}dx - \ln[c_{\rm DL}(x=0,t)]. \tag{35}$$

Equation (35) is the dashed red line in Fig. 7. It shows remarkable correspondence to simulations until time T. We also note that at steady state, for $i < i_{\rm lim}$, Eq. (35) reproduces Eq. (1).

For $t > T$, the depletion front is moving away from the permselective interface. The exact location of the front can be calculated by $c_{\rm DL}(x=x_*,t)=0$ where x_* is the location of the moving depletion front. Mathematically, it is defined by Eq. (29):

$$x_* = 1 - \frac{2}{i} + 2\sum_{m=1}^{\infty}\frac{(-1)^m}{\gamma_m^2}e^{-\gamma_m^2 t}\sin[\gamma_m(1-x_*)]. \tag{36}$$

Four comments are necessary. First, $x_*(t>T)$ needs to be numerically calculated from Eq. (36). From numerical investigation of $c_{\rm DL}(x_*,t)$ it can be shown that for $t > T$ only the $m=1$ mode is non-negligible. Thus, it is relatively simple to calculate $x_*(t>T)$. Second, it is also possible to estimate T for $i > 2$ by requiring that $x_*(t=T)=0$. This yields

$$T \cong -\frac{4}{\pi^2}\ln\left[\frac{\pi^2}{8}\left(1-\frac{2}{i}\right)\right]. \tag{37}$$

Third, at steady state, the location of the depletion front is

$$\tilde{x}_* = x_*(t\to\infty) = 1 - \tfrac{1}{2}i. \tag{38}$$

Fourth, Eq. (38) is similar Eq. (14) in Y09 except for the factor 2. We have defined our current density to be half of the one used in Y09 (there $i_{\rm lim}=1$ while here it $i_{\rm lim}=2$). This difference will be carried throughout this work.

C. Steady-state solution

As shown in Refs. [32,35,36,46] the equation governing steady-state ion transport through a 1D permselective media is

$$\varepsilon^2\left[E_{,xx} - \tfrac{1}{2}E^3 + \tfrac{1}{2}E^2(x=1)E\right] - \tfrac{1}{2}i(x-\tilde{x}_*)E = i/2. \tag{39}$$

Y09 solved this equation for the DL, TL, SCL, and CBL separately. Thereafter, using a clever regularization scheme, Y09 integrates across the entire domain comprising the DL, TL, SCL, and CBL and finds the above-limiting current-voltage response [Y09's Eq. (52)],

$$V(t\to\infty) = \frac{\sqrt{2}\left(\frac{1}{2}i-2\right)^{3/2}}{3\varepsilon i} - \ln\left[4\varepsilon i\left(\tfrac{1}{2}i-1\right)^{1/2}\right] + 2n + \frac{3\gamma}{2} + 0.634, \tag{40}$$

where $\gamma = 0.577\,21$ is Euler's constant and $n = \sinh^{-1}[(i\tilde{x}_*/N)^{1/2}]$. We note a difference between Eq. (40) and Y09's Eq. (52). Yariv did not account for the $-\ln N$ term in Eq. (12) and as a result Y09 has an additional $\ln N$ which has been removed here. As pointed out by Yariv, this equation is similar to that derived by Ben and Chang [32] [their Eq. (3.15)]. See Y09 for a thorough comparison of these two works. For the purpose of this work, it is in fact beneficial to note that Y09 derived each of the terms in Eq. (40) as a function of $\tilde{x}_*$ [Eq. (38)]. In this notation the above-limiting current-voltage response is

$$V(t\to\infty) = \frac{2i^{1/2}\tilde{x}_*^{3/2}}{3\varepsilon} + \ln\left(\frac{1-\tilde{x}_*}{4\varepsilon\sqrt{2i\tilde{x}_*}}\right) + 2n + \frac{3\gamma}{2} + 0.634. \tag{41}$$

Both Eqs. (40) and (41) are identical and are given by the dotted black line in Fig. 7. They indeed show remarkable correspondence at steady state. In the remainder, we will present additional results from Y09 that are needed for our calculations. See Y09 for more details and explicit expressions for the electric fields in each of the four regions.

D. Intermediate times

We return to the time-dependent governing equations and consider the SCL region:

$$c_{{\rm SCL},t} = c_{{\rm SCL},xx} - \tfrac{1}{2}\varepsilon^2\left(E_{\rm SCL}^2\right)_{,xx}, \tag{42}$$

$$-\varepsilon^2(E_{{\rm SCL},t} - E_{{\rm SCL},xx}) = c_{\rm SCL}E_{\rm SCL} + i/2. \tag{43}$$

In the steady state, it was shown that [35,36]

$$E_{\rm SCL} \approx \varepsilon^{-1}E_{\rm SCL,-1} + E_{\rm SCL,0} + \varepsilon E_{\rm SCL,1} + \varepsilon^2 E_{\rm SCL,2} + \cdots . \tag{44}$$

Inserting Eq. (44), which now depends on time, into Eqs. (42) and (43) results in two interesting results. First, Eq. (43) yields to leading order conservation of the electric current density:

$$c_{\rm SCL}E_{\rm SCL} = c_{\rm SCL}\varepsilon^{-1}E_{\rm SCL,-1} = -\tfrac{1}{2}i. \tag{45}$$

This in turn suggests that the leading order term of the concentration in the SCL, c_{SCL}, is linear to $O(\varepsilon)$ [this will be shown shortly—Eq. (54)]. Second, due to the $c_{\rm SCL} = \tilde{c} \sim O(\varepsilon)$ scaling Eq. (42) reduces to

$$\tfrac{1}{2}\varepsilon^2\left(E^2_{\rm SCL}\right)_{,xx} = \tfrac{1}{2}\left(E^2_{\rm SCL,-1}\right)_{,xx} = 0. \tag{46}$$

Thus, remarkably, both leading order equations are steady state. This might appear paradoxical for a time-dependent problem. The resolution to this is that the time dependency of the problem enters via the location of the moving depletion front [Eq. (36)].

The observation that the problem is "quasi" steady state suggests the following ansatz: Replace $\tilde{x}_*$ in Eq. (41) with $x_*(t)$ calculated from Eq. (36). This yields

$$V(t \gg T) = \frac{2i^{1/2}[x_*(t)]^{3/2}}{3\varepsilon} + \ln\left[\frac{1-x_*(t)}{4\varepsilon\sqrt{2ix_*(t)}}\right] + 2n + \frac{3\gamma}{2} + 0.634. \tag{47}$$

This solution is given by the dashed-dotted blue line in Fig. 7. It can be observed that at steady state, as $x_* \to \tilde{x}_*$, we get the expected result that $V(t \gg T) \to V(t \to \infty)$. Also, it appears that the ansatz holds until it fails near the second bend of the simulation curve of Fig. 7. This can be attributed to the fact that in Eq. (47) it has been assumed that there are four fully developed regions (DL, TL, SCL, and CBL). However, perhaps the TL is not fully formed. If that is the case, that would explain why Eq. (47) overpredicts the space charge in the TL. This would increase the conductance in this region—or equivalently decrease the resistance and the resultant voltage.

To support this explanation, we derive the voltage drop across three regions (DL, SCL, and CBL) and neglect the effects of the TL. This potential drop is then

$$\Delta\phi_{\rm 3\ layers} = \Delta\phi_{\rm DL} + \Delta\phi_{\rm SCL} + \Delta\phi_{\rm CBL} - \ln N. \tag{48}$$

Similar to Eq. (32) the potential drop in the DL is calculated from

$$\Delta\phi_{\rm DL}(t) = \int_{x_*}^{1} \frac{i}{2c_{\rm DL}(x,t)}dx, \tag{49}$$

where the bottom integral limit has been modified [relative to Eq. (32)] from 0 to x_*. In the SCL, Y09 gives

$$E_{\rm SCL,-1} = -\sqrt{i(x_*-x)}, \tag{50}$$

$$E_{\rm SCL,0} = -1/[2(x_*-x)]. \tag{51}$$

To leading order, we find that

$$\Delta\phi_{\rm SCL}(t) = -\int_0^{x_*} E_{\rm SCL}dx \cong -\int_0^{x_*}\frac{E_{\rm SCL,-1}}{\varepsilon}dx = \int_0^{x_*}\frac{\sqrt{i(x_*-x)}}{\varepsilon}dx = \frac{2i^{1/2}x_*^{3/2}}{3\varepsilon}. \tag{52}$$

This is the first term in Eq. (47). To find the potential difference in the CBL ($\Delta\phi_{\rm CBL}(t) = -\ln[\tilde{c}_{\rm SCL}(x\to 0)]$), it remains for us to calculate the concentration near the interface,$\tilde{c}_{\rm SCL}(x\to 0)$. The concentration in all three regions is given by Y09

$$c = \tfrac{1}{2}i(x-x_*) + \tfrac{1}{2}\varepsilon^2[E^2 - E^2(x=1)]. \tag{53}$$

Inserting Eqs. (44), (50), and (51) in Eq. (53) yields to leading order

$$c_{\rm SCL} = \sqrt{\frac{i}{x_*-x}}\frac{\varepsilon}{2}, \tag{54}$$

such that $c_{\rm SCL}(x\to 0) = (\varepsilon i^{1/2})/(2x_*^{1/2})$. Then the potential drop [Eq. (48)] is

$$V_{\rm SCL}(t) = \Delta\phi_{\rm 3\ layers} = \int_{x_*}^{1}\frac{i}{2c_{\rm DL}(x,t)}dx + \frac{2i^{1/2}x_*^{3/2}}{3\varepsilon} - \ln\left(\sqrt{\frac{i}{x_*}}\frac{\varepsilon}{2}\right). \tag{55}$$

Note that last term is also reminiscent of a term that appears in Eq. (47). Also, it should be noted that the nonlinear resistance is dominated here by the second term which is of $O(\varepsilon^{-1})$ while the two remaining terms are of order $O(\varepsilon^0)$ and $O(\ln\varepsilon)$. Equation (55) is given by the dotted magenta line in Fig. 7 and shows good correspondence for intermediate times. At larger times, this solution fails where it overpredicts the resistance and the voltage. This can be attributed to the lack of inclusion of the TL.

IV. CONCLUSIONS

This work considers the time evolution of the potential drop across a standard 1D system, whose two ends are a permselective interface and bulk, undergoing concentration polarization for above-limiting currents. To describe the complicated behavior of the potential drop, we note that the structure of the space charge varies in time in a manner which is analogous to how the space-charge varies in the steady state with increasing currents.

For short times, the space charge is highly localized in the EDL. The remaining DL is electroneutral. Utilizing the electroneutral approach of the steady state, we derive the short time approximation for the potential drop [$V(t<T)$, Eq. (35)] which holds until the concentration is completely depleted at the permselective interface.

At steady state, the eSCL comprises three regions (CBL, SCL, and TL). The current-voltage response is then given by Y09's remarkably simply expression [$V(t\to\infty)$, Eq. (41)]. Using an ansatz of replacing steady-state depletion front location $\tilde{x}_*$ with a time-evolving depletion front $x_*(t)$, we

derive the time-evolving version of Eq. (41)—this is Eq. (47) [$V(t \gg T)$].

Leveraging the understandings that the governing equations are quasi steady state once the concentration at the interface is completely depleted, we derive an expression for the potential drop across the system for intermediate times when we assume that the effects of the TL are negligible [$V_{SCL}(t)$, Eq. (55)].

Our overall goal has been to elucidate how the change in the structure of the EDL effects the change in the potential drop. Our three different equations show very good correspondence to the fully coupled numerical simulation (Fig. 7).

It is our hope that this approach can be extended to additional nanofluidic systems that currently suffer from unresolved questions regarding time dependencies, for example, semi-infinite domains, or three-layered systems that account for the behavior within the permselective region as well as the enriched region. Hopefully, this work demonstrates that time-dependent problems in permselective systems might not be as difficult as one might initially assume, and that more effort should be made in addressing these problems.

[1] I. Rubinstein, *Electro-Diffusion of Ions* (SIAM, Philadelphia, 1990).

[2] S. A. Mareev, A. V. Nebavskiy, V. S. Nichka, M. Kh. Urtenov, and V. V. Nikonenko, The nature of two transition times on chronopotentiograms of heterogeneous ion exchange membranes: 2D modelling, J. Membr. Sci. **575**, 179 (2019).

[3] O. A. Rybalkina, K. A. Tsygurina, V. V. Sarapulova, S. A. Mareev, V. V. Nikonenko, and N. D. Pismenskaya, Evolution of current–voltage characteristics and surface morphology of homogeneous anion-exchange membranes during the electrodialysis desalination of alkali metal salt solutions, Membr. Membr. Technol. **1**, 107 (2019).

[4] I. Rubinstein and B. Zaltzman, Electro-osmotically induced convection at a permselective membrane, Phys. Rev. E **62**, 2238 (2000).

[5] L.-J. Cheng and L. J. Guo, Rectified ion transport through concentration gradient in homogeneous silica nanochannels, Nano Lett. **7**, 3165 (2007).

[6] Z. Zhang, S. Yang, P. Zhang, J. Zhang, G. Chen, and X. Feng, Mechanically strong MXene/Kevlar nanofiber composite membranes as high-performance nanofluidic osmotic power generators, Nat. Commun. **10**, 2920 (2019).

[7] Y. Green, Y. Edri, and G. Yossifon, Asymmetry-induced electric current rectification in permselective systems, Phys. Rev. E **92**, 033018 (2015).

[8] D. Brogioli, Extracting Renewable Energy from a Salinity Difference Using a Capacitor, Phys. Rev. Lett. **103**, 058501 (2009).

[9] F. La Mantia, M. Pasta, H. D. Deshazer, B. E. Logan, and Y. Cui, Batteries for efficient energy extraction from a water salinity difference, Nano Lett. **11**, 1810 (2011).

[10] F. H. J. van der Heyden, D. J. Bonthuis, D. Stein, C. Meyer, and C. Dekker, Power generation by pressure-driven transport of ions in nanofluidic channels, Nano Lett. **7**, 1022 (2007).

[11] A. Meller, L. Nivon, and D. Branton, Voltage-Driven DNA Translocations through a Nanopore, Phys. Rev. Lett. **86**, 3435 (2001).

[12] B. Nadler, Z. Schuss, U. Hollerbach, and R. S. Eisenberg, Saturation of conductance in single ion channels: The blocking effect of the near reaction field, Phys. Rev. E **70**, 051912 (2004).

[13] A. Meller, A new tool for cell signalling research, Nat. Nanotechnol. **14**, 732 (2019).

[14] Z. S. Siwy and S. Howorka, Engineered voltage-responsive nanopores, Chem. Soc. Rev. **39**, 1115 (2010).

[15] R. Karnik, R. Fan, M. Yue, D. Li, P. Yang, and A. Majumdar, Electrostatic control of ions and molecules in nanofluidic transistors, Nano Lett. **5**, 943 (2005).

[16] R. Karnik, C. Duan, K. Castelino, H. Daiguji, and A. Majumdar, Rectification of ionic current in a nanofluidic diode, Nano Lett. **7**, 547 (2007).

[17] W. Guan, R. Fan, and M. A. Reed, Field-effect reconfigurable nanofluidic ionic diodes, Nat. Commun. **2**, 506 (2011).

[18] R. Yan, W. Liang, R. Fan, and P. Yang, Nanofluidic diodes based on nanotube heterojunctions, Nano Lett. **9**, 3820 (2009).

[19] Y. Green, Current-voltage response for unipolar funnel-shaped nanochannel diodes, Phys. Rev. E **98**, 033114 (2018).

[20] Y. Qiu, R. A. Lucas, and Z. S. Siwy, Viscosity and conductivity tunable diode-like behavior for meso- and micropores, J. Phys. Chem. Lett. **8**, 3846 (2017).

[21] Y. Green, R. Eshel, S. Park, and G. Yossifon, Interplay between nanochannel and microchannel resistances, Nano Lett. **16**, 2744 (2016).

[22] V. G. Levich, *Physicochemical Hydrodynamics* (Prentice-Hall, New York, 1962).

[23] I. Rubinstein and L. Shtilman, Voltage against current curves of cation exchange membranes, J. Chem. Soc., Faraday Trans. 2 **75**, 231 (1979).

[24] I. Rubinstein and B. Zaltzman, Electro-osmotic slip of the second kind and instability in concentration polarization at electrodialysis membranes, Math. Models Methods Appl. Sci. **11**, 263 (2001).

[25] B. Zaltzman and I. Rubinstein, Electro-osmotic slip and electroconvective instability, J. Fluid Mech. **579**, 173 (2007).

[26] G. Yossifon and H.-C. Chang, Selection of Nonequilibrium Overlimiting Currents: Universal Depletion Layer Formation Dynamics and Vortex Instability, Phys. Rev. Lett. **101**, 254501 (2008).

[27] S. M. Rubinstein, G. Manukyan, A. Staicu, I. Rubinstein, B. Zaltzman, R. G. H. Lammertink, F. Mugele, and M. Wessling, Direct Observation of a Nonequilibrium Electro-Osmotic Instability, Phys. Rev. Lett. **101**, 236101 (2008).

[28] E. V. Dydek, B. Zaltzman, I. Rubinstein, D. S. Deng, A. Mani, and M. Z. Bazant, Overlimiting Current in a Microchannel, Phys. Rev. Lett. **107**, 118301 (2011).

[29] M. B. Andersen, M. van Soestbergen, A. Mani, H. Bruus, P. M. Biesheuvel, and M. Z. Bazant, Current-Induced Membrane Discharge, Phys. Rev. Lett. **109**, 108301 (2012).

[30] C. P. Nielsen and H. Bruus, Transport-limited water splitting at ion-selective interfaces during concentration polarization, Phys. Rev. E **89**, 042405 (2014).

[31] C. P. Nielsen and H. Bruus, Concentration polarization, surface currents, and bulk advection in a microchannel, Phys. Rev. E **90**, 043020 (2014).

[32] Y. Ben and H.-C. Chang, Nonlinear Smoluchowski slip velocity and micro-vortex generation, J. Fluid Mech. **461**, 229 (2002).

[33] G. Yossifon, P. Mushenheim, Y.-C. Chang, and H.-C. Chang, Nonlinear current-voltage characteristics of nanochannels, Phys. Rev. E **79**, 046305 (2009).

[34] K. T. Chu and M. Z. Bazant, Electrochemical thin films at and above the classical limiting current, SIAM J. Appl. Math. **65**, 1485 (2005).

[35] M. Z. Bazant, K. T. Chu, and B. J. Bayly, Current-voltage relations for electrochemical thin films, SIAM J. Appl. Math. **65**, 1463 (2005).

[36] E. Yariv, Asymptotic current-voltage relations for currents exceeding the diffusion limit, Phys. Rev. E **80**, 051201 (2009).

[37] E. Yariv, Improved current-voltage approximations for currents exceeding the diffusion limit, SIAM J. Appl. Math. **71**, 2131 (2011).

[38] E. V. Dydek and M. Z. Bazant, Nonlinear dynamics of ion concentration polarization in porous media: The leaky membrane model, AIChE J. **59**, 3539 (2013).

[39] P. Sistat and G. Pourcelly, Chronopotentiometric response of an ion-exchange membrane in the underlimiting current-range. Transport phenomena within the diffusion layers, J. Membr. Sci. **123**, 121 (1997).

[40] C. Larchet, S. Nouri, B. Auclair, L. Dammak, and V. Nikonenko, Application of chronopotentiometry to determine the thickness of diffusion layer adjacent to an ion-exchange membrane under natural convection, Adv. Colloid Interface Sci. **139**, 45 (2008).

[41] N. Leibowitz, J. Schiffbauer, S. Park, and G. Yossifon, Transient response of nonideal ion-selective microchannel-nanochannel devices, Phys. Rev. E **97**, 043104 (2018).

[42] R. Abu-Rjal, N. Leibowitz, S. Park, B. Zaltzman, I. Rubinstein, and G. Yossifon, Signature of electroconvective instability in transient galvanostatic and potentiostatic modes in a microchannel-nanoslot device, Phys. Rev. Fluids **4**, 084203 (2019).

[43] C. L. Druzgalski, M. B. Andersen, and A. Mani, Direct numerical simulation of electroconvective instability and hydrodynamic chaos near an ion-selective surface, Phys. Fluids **25**, 110804 (2013).

[44] E. A. Demekhin, N. V. Nikitin, and V. S. Shelistov, Direct numerical simulation of electrokinetic instability and transition to chaotic motion, Phys. Fluids **25**, 122001 (2013).

[45] Y. Green and G. Yossifon, Time-dependent ion transport in heterogeneous permselective systems, Phys. Rev. E **91**, 063001 (2015).

[46] A. S. Khair, Concentration polarization and second-kind electrokinetic instability at an ion-selective surface admitting normal flow, Phys. Fluids **23**, 072003 (2011).